Design of Tuneable Damping for Precision Positioning of a Two-Body System

Francesco Cigarini, Ernst Csencsics, Rudolf Saathof, Georg Schitter

Automation and Control Institute (ACIN), TU Wien, Gusshaustrasse 27-29, 1040, Vienna, Austria.
(e-mail: {cigarini, csencsics, saathof, schitter}@acin.tuwien.ac.at)

Abstract: Mechanical decoupling poses a limit to the achievable positioning precision of a two-body system actuated by a single Lorentz actuator. To control such a system, the damping between the two bodies needs to be adjusted to a trade-off value, which allows both high control bandwidth of the directly actuated body and good isolation from environmental vibration. In this paper, hydraulic shock absorbers are employed to tune the damping. An experimental setup of a two-body system is built, with the shock absorbers mounted between the bodies. A higher level of damping of the decoupling mode is observed by using fluids with higher dynamic viscosity. The effectiveness of the proposed solution is confirmed by comparing the theoretical and experimental values of the damping coefficient for different values of the dynamic viscosity.

Keywords: Two-body systems, precision positioning, damping

1. INTRODUCTION

In metrology, nanopositioning and nano-manufacturing, a high control bandwidth is typically desired to achieve high levels of precision (Munnig Schmidt et al., 2014). In most high-precision applications, an additional limit to the attainable system performance is caused by environmental vibrations (Amick et al., 2005). Because of their ability to attenuate such vibrations, low-stiffness actuators such as Lorentz actuators can be employed (Ito and Schitter, 2015). In Lorentz-actuated systems, the achievable control bandwidth is typically limited by higher structural modes of the positioned system (Lee et al., 2007). Such modes commonly arise either from the internal degrees of freedom of the mechanical structure or from the decoupling of its different components, as in the case of multi-body systems (Meirovitch, 2001).

Multi-body systems are used in several high-precision applications. For example, a metrology platform consisting of multiple components is proposed to measure nanoscale material properties in a production environment (Thier et al., 2015). This platform is directly actuated to maintain a constant distance between a sample and a measurement tool, thereby mitigating the effect of ground vibrations. Other examples of multi-body systems are wafer scanners, used for the manufacturing of integrated circuits. Because of the high precision requirement (Butler, 2011), they employ vibration isolation frames, which are typically actuated to counteract external disturbances. These systems consist of complex architectures, including several subsystems, sensors and actuators, which also cause structural resonance modes at a given frequency.

The simplest case of a multi-body system is given by a two-body system, shown in Fig. 1. The system consists of (i) the body S_1 that is directly actuated and (ii) the body S_2 that is mechanically connected to S_1. Such a model represents typical structural modes of the positioned structure, which is also referred to as a decoupling mass (body S2; see Munnig Schmidt et al. (2014)). This results in a combination of a resonance- and an anti-resonance in the system transfer function and typically is a limiting factor for the achievable control bandwidth for feedback operation. Typical countermeasures aim to suppress such unwanted structural modes, e.g. via active damping (Babakhani and Vries, 2010) and overactuation (Schneiders et al., 2003). In such cases additional actuators need to be placed into the structure, leading to higher system as well as control complexity.

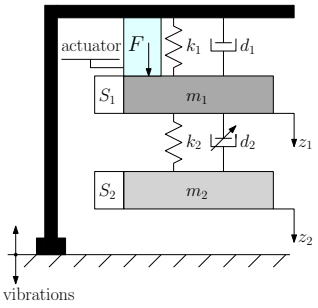

Fig. 1. Schematic model of a two-body system.

In contrast to such strategies, Csencsics et al. (2016) utilizes a resonance mode on purpose. In this approach, the position of the two-body system is controlled via a single Lorentz actuator. This method takes advantage of the second resonance mode of the system (known in this case as decoupling mode) to actively control S_1 with high bandwidth, while isolating S_2 from environmental

Post-print version of the article: Francesco Cigarini, Ernst Csencsics, Rudolf Saathof and Georg Schitter, "Design of Tuneable Damping for Precision Positioning of a Two-Body System," *Proceedings of the 7th IFAC Symposium on Mechatronic Systems*, pp. 222-227, 2016. DOI: 10.1016/j.ifacol.2016.10.554

vibrations. To achieve this however, high damping of the antiresonance and of the second resonance peak is needed. An undamped antiresonance would in fact impair control at this frequency and lead to undesirable high control effort. Additionally, an undamped decoupling resonance may cause extensive excitation of S_2 at this frequency, e.g. due to external disturbances. This shows that the damping d_2 between S_1 and S_2 is an important design parameter, as by changing its value the damping of the antiresonance dip and of the resonance peak can be tuned.

To increase d_2, viscoelastic free-layer and constrained-layer damping can be directly applied to the mechanical connections between S_1 and S_2 (Jones, 2001). In this case, the models describing the damping coefficient are computational-intensive and often require the use of Finite Element Method (Vasques et al., 2010), leading to high design complexity. Eddy-current dampers (Wesselingh, 2015), as well as electrorheological (Holzmann et al., 2009) and magnetorheological dampers (Lai and Liao, 2002) allow to adjust the level of damping by regulating the intensity of an external electromagnetic field. In this case the drawback is the need for an external energy source, with the consequence of increased system complexity.

However, a suitable solution can be found in hydraulic shock absorbers (Dixon, 2008). In this case, the damping coefficient can be determined as a linear function of the viscosity of the fluid used (Rao, 2016). This allows to tune the level of damping by simply changing the fluid, without the need for an external energy source. Because of these advantages, hydraulic shock absorbers are proposed in this paper to introduce damping in a two-body system.

The paper is organized as follows. In Section 2, the experimental setup of the two-body system is presented. In Section 3 the dynamics of the setup are simulated. In Section 4, the design of the shock absorber is presented and the dependence of the damping coefficient on the dynamic viscosity coefficient is shown. In Section 5, the frequency response of the two-body system is measured for fluids of different viscosity and the tuneability of the damping is demonstrated. The paper is concluded in Section 6.

2. SYSTEM DESCRIPTION

In order to demonstrate the tuneability of the damping, an experimental setup of a two-body system is built (see Fig. 2 and Fig. 3). It consists of a body S_1, connected via leaf springs (CuZn37 brass, thickness 0.4 mm) to mechanical ground and to a body S_2. Two hydraulic shock absorbers are installed between the two bodies to introduce additional damping in the system.

The system is actuated by a Lorentz actuator (AVM12-6.4, Akribis Systems, Singapore), which is installed underneath S_1. The coil of the actuator is stiffly connected to S_1 (see Fig. 2(a)), while the permanent magnet is fixed to mechanical ground. The actuator is driven by a custom-made voltage amplifier. For measuring the position of the two bodies, a single-point vibrometer (OFV-534, Polytec GmbH, Hörsching, Germany) is focused on the center of S_1 and S_2, respectively. For data acquisition, a system analyzer (3563A, Hewlett-Packard, Palo Alto, USA) is used.

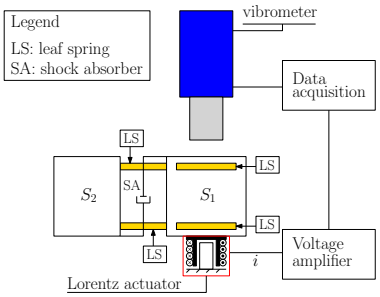

(a) Side view of the experimental setup.

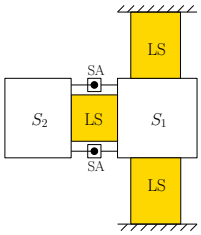

(b) Top view of the experimental setup.

Fig. 2. Schematic (a) side and (b) top view of the experimental setup.

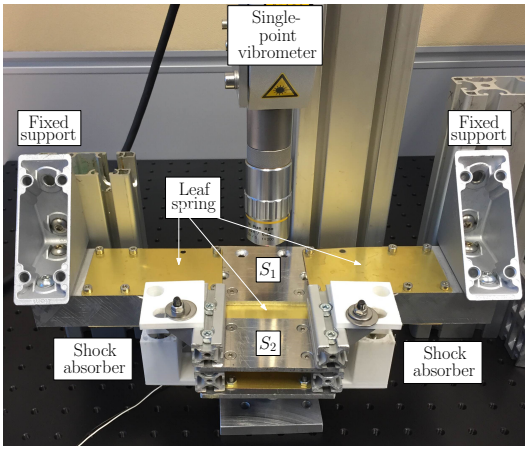

Fig. 3. Experimental setup of the two-body system.

3. SYSTEM ANALYSIS

3.1 Dynamic model

The lumped-mass model of the experimental setup is shown in Fig. 1. The masses m_1 and m_2 represent the mass of S_1 and S_2, respectively. The spring constants k_1 and k_2 represent the stiffness of the leaf springs connecting S_1 to mechanical ground and to S_2, respectively. The damping coefficient d_1 represent the internal damping of the leaf springs connecting S_1 to mechanical ground. The damping coefficient d_2 results from both the internal damping of the leaf springs connecting the two bodies and the tuneable

Post-print version of the article: Francesco Cigarini, Ernst Csencsics, Rudolf Saathof and Georg Schitter, "Design of Tuneable Damping for Precision Positioning of a Two-Body System," *Proceedings of the 7th IFAC Symposium on Mechatronic Systems*, pp. 222-227, 2016. DOI: 10.1016/j.ifacol.2016.10.554

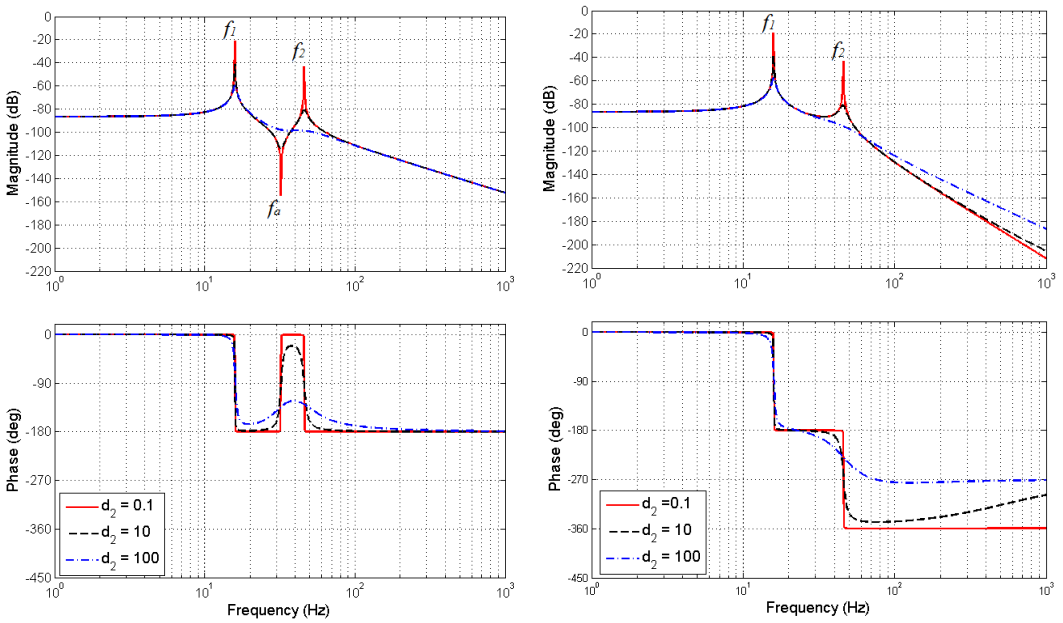

(a) Body S_1 (b) Body S_2

Fig. 4. Simulated frequency responses plots of (a) $G_1(s)$ and (b) $G_2(s)$ for different values of the damping coefficient d_2. The plots show a first resonance peak at $f_1 \simeq 16$ Hz, followed by the antiresonance dip of $G_1(s)$ at $f_a \simeq 32$ Hz and the decoupling resonance peak at $f_2 \simeq 46$ Hz. As the value of d_2 increases, the damping of the antiresonance dip and of the decoupling resonance peak increases, while the decoupling effect is reduced at higher frequencies, with the magnitude slope of $G_2(s)$ raising to -60 $^{\text{dB}}/_{\text{decade}}$ and the phase to $-270°$.

damping introduced by the shock absorbers. The system is actuated by a force F that is exerted on S_1 by the Lorentz actuator. The coordinates z_1 and z_2 represent the position of S_1 and the S_2, respectively.

From the lumped mass model, the following equations of motion are derived:

$$\begin{aligned} m_1\ddot{z}_1(t) = F - k_1 z_1(t) - k_2(z_1(t) - z_2(t)) \\ - d_1\dot{z}_1(t) - d_2(\dot{z}_1(t) - \dot{z}_2(t)), \quad (1) \\ m_2\ddot{z}_2(t) = k_2(z_1(t) - z_2(t)) + d_2(\dot{z}_1(t) - \dot{z}_2(t)). \quad (2) \end{aligned}$$

By solving (1) and (2), the transfer functions $G_1(s) = Z_1(s)/F(s)$ of S_1 and $G_2(s) = Z_2(s)/F(s)$ of S_2 are obtained:

$$G_1(s) = \frac{m_2 s^2 + d_2 s + k_2}{m_1 m_2 s^4 + D_3 s^3 + D_2 s^2 + D_1 s + k_1 k_2}, \quad (3)$$

$$G_2(s) = \frac{d_2 s + k_2}{m_1 m_2 s^4 + D_3 s^3 + D_2 s^2 + D_1 s + k_1 k_2}, \quad (4)$$

with:

$$\begin{cases} D_1 = d_1 k_2 + d_2 k_1, & (5a) \\ D_2 = d_1 d_2 + k_1 m_2 + k_2 m_1 + k_2 m_2, & (5b) \\ D_3 = d_1 m_2 + d_2 m_1 + d_2 m_2. & (5c) \end{cases}$$

Fig. 4 shows the frequency response plot of $G_1(s)$ and $G_2(s)$ for the values listed in Table 1 (corresponding to the dimensional parameters of the experimental setup) and three different values of the damping coefficient d_2.

Table 1. Parameters of the two-body system

Parameter	Value	Unit
m_1	1.1	kg
m_2	0.8	kg
k_1	2.1 $\times 10^4$	N/m
k_2	3.4 $\times 10^4$	N/m
d_1	0.010	N s/m

Both plots show a pronounced first resonance frequency at $f_1 \simeq 16$ Hz, corresponding to the suspension mode of the system. Around this frequency, the phase of $G_1(s)$ and $G_2(s)$ changes to $-180°$. Above f_1, the dynamics of the system depend on the value of d_2. For the case of low damping ($d_2 = 0.10$ N s/m), $G_1(s)$ shows a pronounced antiresonance dip at $f_a \simeq 32$ Hz. At this frequency, the force is nearly completely transferred from the actuator to S_2, while S_1 remains nearly stationary. At $f_2 \simeq 46$ Hz the second resonance mode occurs. Above this frequency, $G_1(s)$ shows a magnitude slope of -40 $^{\text{dB}}/_{\text{decade}}$ and a phase of $-180°$, while $G_2(s)$ shows a magnitude slope of -80 $^{\text{dB}}/_{\text{decade}}$ and a phase of $-360°$. This inability of S_2 to follow the movement of S_1 is called decoupling of the body S_2 (Munnig Schmidt et al., 2014). Above f_2, the mass line of $G_1(s)$ is vertically lifted to a higher level respect to before the decoupling. This vertical shift depends on the

Post-print version of the article: Francesco Cigarini, Ernst Csencsics, Rudolf Saathof and Georg Schitter, "Design of Tuneable Damping for Precision Positioning of a Two-Body System," *Proceedings of the 7th IFAC Symposium on Mechatronic Systems*, pp. 222-227, 2016. DOI: 10.1016/j.ifacol.2016.10.554

ratio of $m_1 + m_2$ to m_1 and represents a design parameter that has the potential to reduce the energy consumption of the entire system.

3.2 Influence of the damping coefficient d_2

As shown in Fig. 4, a high damping coefficient d_2 corresponds to less pronounced antiresonance dip and decoupling reasonance peak. These are both desirable conditions when designing a controller to position S_1 with a bandwidth above the decoupling frequency (Csencsics et al., 2016). A pronounced antiresonance dip could be compensated by a lowly-damped resonance in the controller, which however may lead to a saturating controller output. Furthermore, a pronounced decoupling resonance peak may cause extensive excitation of S_2 around f_2 due to external disturbances. Additionally, a high value of d_2 will cause the phase of $G_1(s)$ above f_2 to rise, allowing a higher phase margin of the controlled system. On the other side, as the value of d_2 increases, the decoupling effect is reduced, with the magnitude slope of $G_2(s)$ raising to -60 $^{\mathrm{dB}}/_{\mathrm{decade}}$ and the phase to $-270°$. This effect is caused by a damping-related shift of the zero of $G_2(s)$, which can be calculated from (4) as:

$$f_z = \frac{1}{2\pi}\frac{k_2}{d_2}. \tag{6}$$

For higher values of d_2, the zero is moved to lower frequencies, causing the phase and magnitude of $G_2(s)$ to raise. This leads to a reduction of the decoupling effect and an increased risk of excitation of potential structural modes of S_2.

These considerations suggest that d_2 should be tuneable to a trade-off value to facilitate the control design while preserving the decoupling. As discussed in the next section, this can be achieved by employing hydraulic shock absorbers.

4. DESIGN OF THE HYDRAULIC SHOCK ABSORBERS

A schematic cross-section view of the shock absorbers is shown in Fig. 5. It consists of a cylinder, which is directly installed on S_1, and a piston, which is installed on S_2 via a piston holder. A disk (outer diameter D_d) is mounted on the piston and positioned inside the cylinder (inner diameter D_c), which is filled with silicon oil (Polydimethylsiloxane, PDMS) for tuning the damping coefficient.

Below the antiresonance frequency f_a, S_1 and S_2 move in phase and no relative motion is present inside the shock absorbers. Above f_a, the relative motion of S_1 and S_2 causes the piston to slide inside the cylinder, moving the damping fluid. Because of the resistance of the fluid to motion, a counterforce $F = d_2 \cdot v$ is exerted on the moving parts, directly proportional to the velocity v and to the damping coefficient d_2. Under the assumption of a perfect Newtonian fluid, d_2 is calculated from the dimensional parameters of the shock absorber and the dynamic viscosity μ of the damping fluid (Rao (2016)).

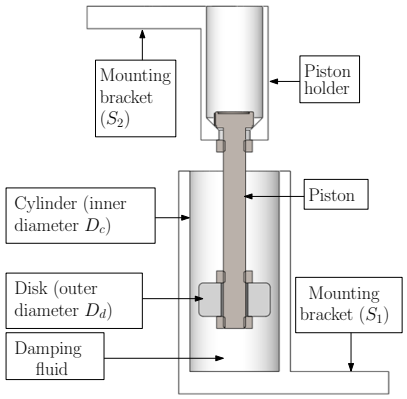

Fig. 5. Schematic cross section view of the shock absorber.

$$d_2 = d_{2i} + n_d \cdot \mu \left[\frac{3\pi}{4} \frac{D_d^3}{D_g^3} L \cdot \left(1 + 2\frac{D_g}{D_d} \right) \right], \tag{7}$$

where d_{2i} is the internal damping of the leaf springs connecting the two bodies, $n_d = 2$ is the number of employed shock absorbers and L is the thickness of the disk. Assuming that the symmetry axes of the piston and of the cylinder are collinear, the gap D_g between the disk and the inner walls of the cylinder is calculated as $D_g = (D_c - D_d)/2$.

The design parameters of the shock absorber are listed in Table 2. These values are chosen in respect of the dimensional constraints of the setup to achieve a high value of d_2.

As it can be seen from (7), the damping coefficient d_2 is directly proportional to the value of the dynamic viscosity μ of the fluid used. This means that by changing the type of fluid (and hence the viscosity), the damping coefficient can theoretically be tuned to the desired value. To prove this, various silicon oils, all with different dynamic viscosity, are used to tune the damping in the system.

Table 2. Dimensional parameters of the shock absorber

Parameter	Value (mm)
D_c	19.5
D_d	12.9
D_g	3.3
L	7.5

5. EXPERIMENTAL RESULTS

The parameters of $G_1(s)$ and $G_2(s)$ are fitted to the measured frequency responses, relating the displacements of S_1 and S_2 to the force exerted by the Lorentz actuator. To measure the frequency responses, the input of the voltage amplifier is considered as the system input and the positions z_1 and z_2 are considered as the system outputs. The positions are measured using a single-point vibrometer (OFV-534, Polytec GmbH, Hörsching, Germany) and the frequency response plots are recorded with a system analyzer (3563A, Hewlett-Packard, Palo Alto, USA). The electrical system of the Lorentz actuator, i.e. the conversion from voltage to current, has a relatively high cut-off

Post-print version of the article: Francesco Cigarini, Ernst Csencsics, Rudolf Saathof and Georg Schitter, "Design of Tuneable Damping for Precision Positioning of a Two-Body System," *Proceedings of the 7th IFAC Symposium on Mechatronic Systems*, pp. 222-227, 2016. DOI: 10.1016/j.ifacol.2016.10.554

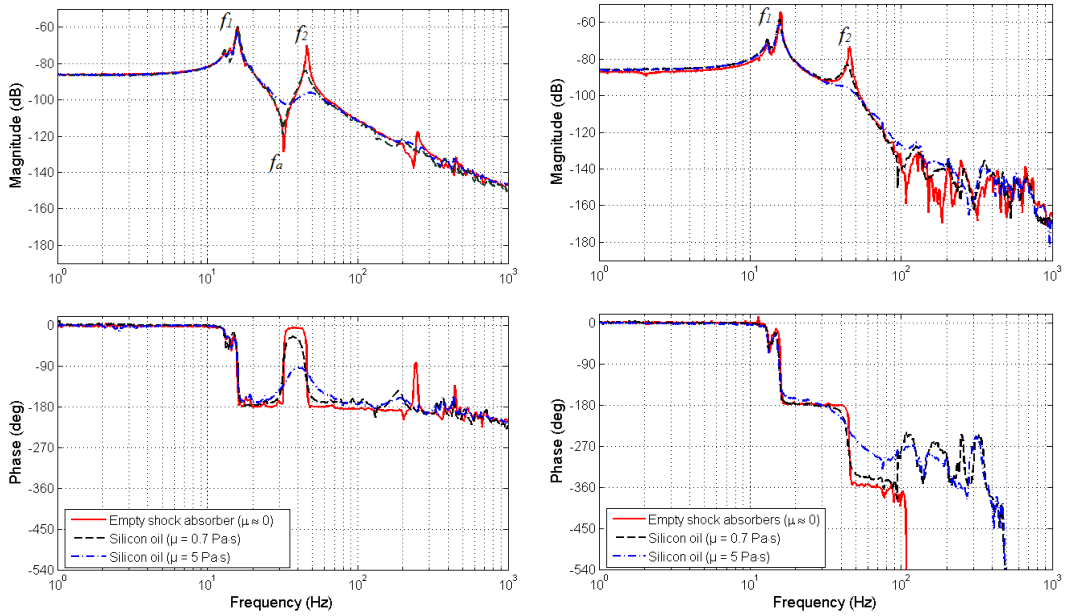

(a) Body S_1 (b) Body S_2

Fig. 6. Measured frequency response plots, relating the displacement of (a) S_1 and (b) S_2 to the force exerted by the Lorentz actuator for different values of the dynamic viscosity μ.

frequency of ca. 2 kHz, while the voltage amplifier has a bandwidth of ca. 50 kHz. Both these frequencies are much higher than the investigated upper frequency limit of ca. 1 kHz.

Table 3 lists the fitted values of d_2 for the five different fluids used. For $\mu \leq 7$ Pa s, d_2 increases with higher values of the dynamic viscosity.

Table 3. Measured damping coefficient d_2 for different values of the dynamic viscosity μ

Damping fluid	μ (Pa s)	d_2 (N s/m)
Air	0	2
Silicon oil 1	0.7	5
Silicon oil 2	3	38
Silicon oil 3	5	55
Silicon oil 4	7	100
Silicon oil 5	10	90

Fig. 7 shows the measured values of d_2 plotted against the dynamic viscosity μ. The values are compared to the simulated curve obtained from the model (7). In the low-viscosity range, i.e. $\mu \leq 5$ Pa s, good agreement can be observed between the measured and simulated values of d_2. In the high-viscosity range a divergence is observed, probably due to the deviation of PDMS from an ideal Newtonian fluid (Kökuti et al., 2011).

Fig. 6 shows the measured frequency response plots for three of the five cases listed in Table 3. The suspension mode of the system can be observed at $f_1 \simeq 16$ Hz, followed by the antiresonance dip at $f_a \simeq 32$ Hz for S_1 and the decoupling resonance peak at $f_2 \simeq 46$ Hz. For higher frequencies, additional dynamics can be observed, likely

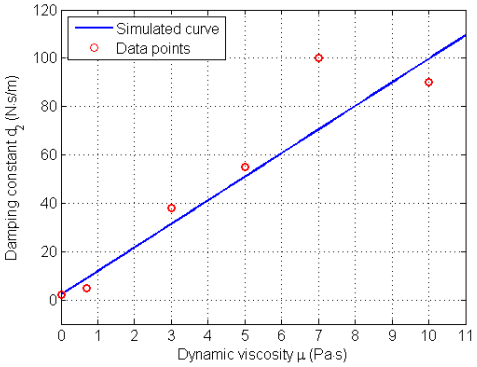

Fig. 7. Damping coefficient d_2 as a function of the dynamic viscosity μ. The solid line represents the simulated curve (7), while the circles represent the measured values of the damping coefficient.

resulting from structural modes of the outer body. Small changes in the frequency of the antiresonance and the decoupling resonance can also be observed for different measurements. This is likely due to the assembly precision of the setup, as the shock absorbers require disassembling and reassembling every time for changing the damping fluid.

As fluids with higher μ are used, the measured frequency response plots show higher damping of both the antiresonance dip and the decoupling resonance peak. Fig. 8

Post-print version of the article: Francesco Cigarini, Ernst Csencsics, Rudolf Saathof and Georg Schitter, "Design of Tuneable Damping for Precision Positioning of a Two-Body System," *Proceedings of the 7th IFAC Symposium on Mechatronic Systems*, pp. 222-227, 2016. DOI: 10.1016/j.ifacol.2016.10.554

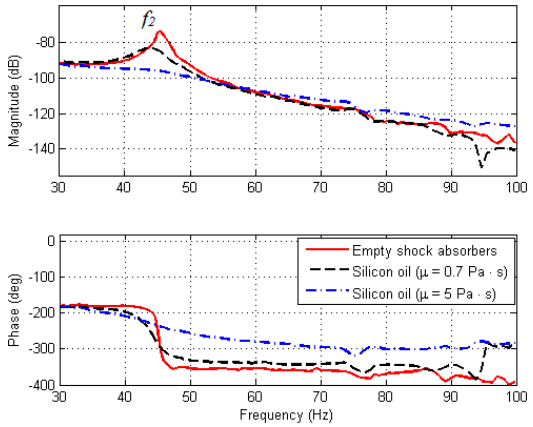

Fig. 8. Zoom of Fig. 6(b) around the decoupling frequency (linear frequency scale).

shows a zoom of Fig. 6(b) around the decoupling frequency f_2. Above f_2, an increase of both the magnitude slope and the phase can be noticed for increasing values of μ. This signifies a reduction of the decoupling effect, in good agreement with what discussed in Section 3.

The presented results demonstrate that shock absorbers can be employed to tune the damping between the two bodies. In the low-viscosity range, the value of the damping coefficient can be estimated by the analytical model (7). As a result, the height of the antiresonance dip and the decoupling resonance peak can be adjusted, thereby improving the controllability, as discussed in Section 1.

6. CONCLUSION

In this paper, the controllability of an underactuated two-body system is improved by directly shaping its dynamics. For this purpose, tuneable damping is introduced between the bodies via hydraulic shock absorbers. In this case, the damping coefficient can be analytically determined from the dimensional parameters of the shock absorbers and the dynamic viscosity of the damping fluid. The tuneability of the damping is validated by measuring the frequency responses of an experimental setup, where various damping fluids are used inside the shock absorbers. The experimental results show that the value of the damping coefficient changes with the viscosity of the damping fluid, in good agreement with the analytical model.

ACKNOWLEDGEMENTS

The authors thank Prof. Robert Munnig Schmidt from TU Delft, as well as Severin Unger and Dr. Shingo Ito from TU Wien for the fruitful discussions. The research work is funded by the EU commission under the FP7 NMP Programme, project title aim4np, grant number 309558.

REFERENCES

Amick, H., Gendreau, M., Busch, T., and Gordon, C. (2005). Evolving criteria for research facilities: I - vibration. In *Proc. SPIE 5933: Buildings for Nanoscale Research and Beyond*, volume 593303, 1 – 13.

Babakhani, B. and Vries, T.J.D. (2010). Active damping of the 1d rocking mode. In *International Conference on Mechatronics and Automation (ICMA)*, 1370–1375.

Butler, H. (2011). Position control in lithographic equipment. *IEEE Control System Magazine*, 28–47.

Csencsics, E., Thier, M., Siegl, P., and Schitter, G. (2016). Mechatronic design of an active two-body vibration isolation system, in press. In *7th IFAC Symposium on Mechatronic Systems & 15th Mechatronics Forum International Conference*, in press.

Dixon, J.C. (2008). *The Shock Absorber Handbook*. SAE International.

Holzmann, K., Kemmetmüller, W., Kugi, A., Stork, M., Rosenfeldt, H., and Schneider, S. (2009). Modeling and control of an off-road truck using electrorheological dampers. *Journal of Physics: Conference Series*, 149, 1 – 4.

Ito, S. and Schitter, G. (2015). Comparison and classification of high-precision actuators based on stiffness influencing vibration isolation. *IEEE/ASME Transactions on Mechatronics*, 21(2), 1169 – 1178.

Jones, D.I.G. (2001). *Handbook of viscoelastic vibration damping*. John Wiley and Sons.

Kökuti, Z., Kokavecz, J., Czirják, A., Holczer, I., Danyi, A., Gábor, Z., Szabo, G., Pézsa, N., Ailer, P., and Palkovics, L. (2011). Nonlinear viscoelastic and thixotropy of a silicone fluid. *Annals of Faculty of Engineering Hunedoara - International Journal of Enginnering*, IX(2), 177–180.

Lai, C.Y. and Liao, W.H. (2002). Vibration control of a suspension system via a magnetorheological fluid damper. *Journal of Vibration and Control*, 8(4), 527–547.

Lee, D.J., Song, M.G., Kim, C., Park, N.C., Park, Y.P., Onagi, N., and Akanuma, G. (2007). Improvement of dynamic characteristics for symmetric-type slim optical pickup actuator by changing coil shape. *IEEE Transactions on Magnetics*, 43(2), 808–810.

Meirovitch, L. (2001). *Fundamentals of Vibrations*. Mc Graw Hill.

Munnig Schmidt, R., Schitter, G., Rankers, A., and van Eijk, J. (2014). *The Design of High Performance Mechatronics, 2nd revised edition*. IOS Press BV.

Rao, S.S. (2016). *Mechanical Vibrations*. Prentice Hall.

Schneiders, M.G., van de Molengraft, M.J.G., and Steinbuch, M. (2003). Introduction to an integrated design for motion systems using over-actuation. In *Proceedings of the European Control Conference 2003 (ECC)*, 3249 – 3254.

Thier, M., Saathof, R., Hainisch, R., and Schitter, G. (2015). Vibration compensation platform for robot-based nanoscale measurements. In *euspen's 15th International Conference Exhibition*, 211–212.

Vasques, C.M.A., Moreira, R.A.S., and Rodrigues, J.D. (2010). Viscoelastic damping technologies-part i: Modeling and finite element implementation. *Journal of Advanced Research in Mechanical Engineering*, 1(2), 76–95.

Wesselingh, J. (2015). Electromagnetic dampers in precision machines. In *euspen's 15th International Conference Exhibition*, 279–280.